CHAPTER IV
PREPARATION OF GRAPHENE/NATURAL RUBBER COMPOSITE FOR COMPLIANT ELECTRODE APPLICATION

4.1 Abstract

A compliant electrode is a stretchable electronic device that retains good conductivity under stretching. It has been used in various electro-actuating applications that require large deformations under electrical activated energy. The purpose of this work was to fabricate the compliant electrode possessing high electrical conductivity and good mechanical properties. Due to the excellent mechanical properties of natural rubber (NR), it was used as a matrix for preparing a compliant electrode. Graphene is one of many innovative new conductive fillers that provides excellence electrical conductivity. In order to investigate its mechanical properties and electrical conductivity, an experiment was carried out by using a melt rheometer in tension mode. Both mechanical and electrical properties were improved by introducing graphene into the matrix. Despite the strain of NR films reaching 80%, the films were able to maintain electrical conductivity values with very low drop offs. The highest electrical conductivity was obtained from the 35.0 %v/v graphene/NR composite which was greater than the DANFOSS commercial compliant electrode. In conclusion, a graphene /NR composite was shown here as a promising material for using as a compliant electrode.

Keywords: Natural rubber; Graphene; Compliant electrode; Flexible material

4.2 Introduction

A compliant electrode is a stretchable electronic device that retains good conductivity under stretching. It has been used in various electro-actuating applications that require large deformations under electrical activated energy (Pelrine *et al.*, 2000). Utilization of compliant electrode has been increasing in the last decade for effective performances of electro-active polymers (EAPs).

In the recent work compliant electrode has been fabricated from various elastic materials, polydimethylsiloxane (PDMS) elastomer (Kujawski *et al.*, 2010), copolymer of tert-butyl acrylate (TBA) and acrylic acid (AA) (poly(TBA-co-AA)) (Yun *et al.*, 2012), and silicone rubber (Kim *et al.*, 2012). The requirements of compliant electrode from literature review were high conductivity (more than 0.1 S/m), sustainablity of conductivity during repeated deformation cycles, and being highly compliant (i.e. Young's modulus <100 MPa) (Delille *et al.*, 2006).

According to requirements of compliant electrode, natural rubber (NR) is a candidate as a matrix of compliant electrode. It is well known to be the most excellent rubbery material having outstanding mechanical properties (Arayapranee *et al.*, 2008) and (Bhattacharyya *et al.*, 2008). Moreover, Thailand is one of the leading NR producers in the world. The natural rubber product is more than 3 million tons per year. The growing productions continued to increase from 3.05 million tons per year in 2007 up to 3.56 million tons in 2011, a 16.8 percentage increase (Manmoun, 2013). In 2012, the rubber production increased to 3.6 million tons, a 8.25 percentage increase (Sincharoenkul, 2012). So, adding value to the Thai NR through the production of compliant electrodes directly benefits Thailand's economy. However, NR is an insulating material and electrical properties can be improved by introducing various conductive fillers.

An enhancement of electrical conductivity can be served by various methods. Metal fillers embedded in polymer matrices are, for example, an epoxy resin (ER) and poly(vinyl chloride) (PVC) filled with copper and nickel powders (Mamunya *et al.*, 2002), conductive polymer blending as a polypyrrole/polypyrrole coated short nylon (Pramila Devi *et al.*, 2013), and the conventional conductive fillers such as a carbon based particle that are widely used in polymer composite

(Sengupta *et al.*, 2011). They are many types of carbon based filler such as carbon black, carbon nanotubes, fullerene, graphite, and graphene.

Graphene is one atom thick, two dimentional honey comb lattice material and it is an ideal candidate as a high-power and high-energy material (Krishnamoorthy *et al.*, 2013). Wang et al. (2007) studied the performance of graphene compared with the other conventional nanofillers (nanoclay, carbon nanotube, ethylene glycol). It was found that graphene has higher surface area, larger aspect ratio, greater tensile strength, higher thermal conductivity and electrical conductivity, better transparency and flexibility (Wang *et al.*, 2007). Luong et al.(2011) studied the mechanical properties of polyimide/graphene composite, they found that Young's modulus of the composite film was dramatically increased from 1.8 GPa to 2.3 GPa and tensile strength was increased from 122 MPa to 131 MPa by adding 0.38 wt% of graphene (Luong *et al.*, 2011). Kim et al. (2011) prepared multi-layers graphene/styrene butadiene rubber nanocomposite and studied the electrical conductivity. They reported that the electrical conductivity of the composite was increased from 4.5×10^{-13} S/cm to 4.5×10^{-7} S/cm with a corresponding increase of graphene from 0.5 wt% to 5 wt% (Kim *et al.*, 2011).

The purpose of this work was to fabricate the compliant electrode possessing high electrical conductivity and good mechanical properties based on graphene as a conductive filler and NR as a matrix. Mechanical and electrical properties were evaluated in terms of graphene concentration and carried out by using the melt rheometer in tension mode. The performances of graphene/NR composites were directly compared with the commercial DANFOSS compliant electrode.

4.3 Experimental

4.3.1 Chemicals and Materials

Double centrifuge natural rubber latex (concentrated latex, 60 % of dry rubber content) was obtained from Thai Eastern Rubber Co., Ltd. Graphene multilayers (commercial grade) having particle dimeter < 2μm was purchased from XG Sciences (USA). TWEEN 80 as a surfactant, 2-methyl-4'-(methylthio)-2 mor-

pholinopropiophenone (MMMP) as a photo-initiator, and trimethylol-propane 3-mercaptopropionate (TMPTMP) as a crosslinker were contributed from Sigma Aldrich. Toluene (reagent grade) was obtained from Carlo ERBA. Deionized water was used in all the experiments. All of reagents was used without further purification.

4.3.2 Preparation of Graphene/NR Composite

TMPTMP concentration was varied at 0.1, 0.5, 1.0, 2.0, 3.0, 5.0, 7.0, 10.0, 15.0, and 20.0 %v/v of NR. The MMMP concentration was set up to be at 3:1 ratio of TMPTMP. First, TMPTMP and MMMP were mixed together with magnetic stirrer until homogenous. The TWEEN 80 (1.0 %v/v) was added into 20 ml DI water and magnetically stirred for 5 min. Graphene was slowly added in TWEEN 80 solution to make a graphene solution. The mixture of TMPTMP and MMMP was added into latex and stirred until homogenous, to be called the latex mixture. Lastly, the graphene solution was added to the latex mixture. The compounded latex was magnetically stirred for 15 min. before curing with UV radiation. The NR film and its composite were investigated under the effects of crosslinking concentration, crosslinking time, and graphene concentration.

4.3.3 Characterizations of Graphene/NR Composite

Raman spectroscope was used to verify graphene multilayers due to the ability to identify and characterize all the members of the carbon family. The indication of graphene was measured by the raman spectroscopy (NT-MDT, NTEGRA Spectra) with 632.8 nm excitation laser, objective lens 100x and accumulate time 60s from National Nanotechnology Center.

The wide angle X-ray diffraction microscope (XRD) was used to study the crystal structure below the nanometer scale. The CuK-alpha radiation source was operated at 40 kV/30 mA. K-beta filter was used to eliminate interference peak. Divergence slit and scattering slit 0.5 deg together with 0.3 mm of receiving slit were set on the instrument.

The crosslink density of NR films was measured by following ASTM D6814-02. The dried rubber sheets were prepared by casting the latex on glass plates and cured under UV radiation at various crosslinking times and crosslinking ratios.

The thin films were cut into small pieces (1 cm^2) and then immersed in toluene (150 mL) until the swelling reached the equilibrium (3 days). The mole percent uptake of solvent, weight loss, and crosslinking density of crosslinked NR were calculated from the following equations:

$$\text{Mole percent uptake of solvent} = \frac{\frac{w_t - w_0}{w_0}}{M_w} \times 100 \tag{4.1}$$

where w_0 and w_t are the weights of dried and swollen samples, respectively. M_w is the molar mass of toluene (92.14 g mol^{-1}).

$$\% \, Weight \, loss = \frac{M_i - M_d}{M_i} \times 100 \tag{4.2}$$

where M_i and M_d are the weight of dried rubber before and after soaking in toluene.

$$v_e = \frac{-[ln(1 - V_r) + V_r + \chi_1 V_r^2]}{[V_1(V_r^{\frac{1}{3}} - V_r)/2]} \tag{4.3}$$

where V_e is effective number of chains in a real network per unit volume, V_r is volume fraction of polymer in a swollen network in equilibrium with pure solvent and is calculated as:

$$V_r = \frac{Weight \, of \, dry \, rubber/density \, of \, dry \, rubber}{\frac{Weight \, of \, dry \, rubber}{Density \, of \, dry \, rubber} + \frac{Weight \, of \, solvent \, absorbed \, by \, sample}{Density \, of \, solvent}} \tag{4.4}$$

where χ_1 is polymer-solvent interaction parameter (0.391) and V_1 is molecular volume of solvent.

The mechanical and electrical properties of pure NR and composite films were measured by the melt rheometer (Rheometric scientific, Ares) with the extensional fixture at room temperature. In this experiment, the transient mode was applied and the stress was monitored during stretching. To evaluate the electrical conductivity, the DC voltage was applied with DC power supply (Instek, GFG 8216A) connected with a digital multimeter (Tektronix, CDM 250) to monitor the voltage input. The electrical conductivity during stretching was calculated through the following equation:

$$\sigma = \frac{1}{R} \times \frac{l}{A} = \frac{I}{V} \times \frac{l}{A} \qquad (4.5)$$

where σ is the electrical conductivity (S/cm), R is the resistivity ($\Omega \times$cm), l is the length of specimen (cm), A is the cross-section area of specimen (cm^2), I is the current (Ampere), and V is the applied voltage (Volt).

In addition, the length and area of specimen depend on the stretching which were calculated based on the incompressible material via the following equations:

$$\gamma = -\frac{\varepsilon_{22}}{\varepsilon_{11}} = -\frac{\varepsilon_{33}}{\varepsilon_{11}} = 0.5 \qquad (4.6)$$

$$t_x = t_0(1 - \epsilon_{33}) = t_0(1 + 0.5\epsilon_{11}) \qquad (4.7)$$

$$w_x = w_0(1 - \epsilon_{33}) = w_0(1 + 0.5\epsilon_{11}) \qquad (4.8)$$

$$l_x = l_0(1 + \varepsilon_{11}) \qquad (4.9)$$

$$\epsilon_{11} = \frac{\Delta l}{l_0} = \frac{l_x - l_0}{l_0} \qquad (4.10)$$

where γ is the Possion ratio (for rubber = 0.5), $\varepsilon_{11,22,33}$ are the strains in x, y, z axes, t is the thickness of specimen (cm), w is the width of specimen (cm), l is the length of specimen (cm). Subscript x means any strain, and subscript 0 means at strain = 0.

A field-emission scanning electron microscope (FE-SEM, JSM-7001F) was used to examine the morphological structure and to determine the dispersion of the graphene in the NR matrix. The film was placed on the holder with an adhesive tape and coated with a thin layer of gold using an ion sputtering device for 100 sec prior to observation under FE-SEM. The SEM images were investigated by using an acceleration voltage of 20 kV with a magnification in the range of 2k - 60k times.

The topology of the composite was obtained by using the atomic force microscope (AFM, Park System, XE-100) in air under ambient conditions. For the

conventional AFM, the non-contact mode was operated with the cantilever (NSC36) tapping at scan rate of 0.5 Hz, applied Z-servo gain of 10, and scanning area of 2 μm^2.

4.4 Result and Discussion

4.4.1 Characterizations of Graphene Multilayers

The Raman spectroscopy is a powerful characterization technique of all types of carbon nanostructures. The main features in the Raman spectra of graphene are called D and G peaks, which are present at around 1329 and 1575 cm^{-1}, respectively, as shown in Figure 4.1. The G peak represents the bond stretching of all pairs of sp^2 atoms in both rings and chains. The D peak refers to the breathing modes of sp^2 atoms in the six angles rings (Ferrari, 2007). Another peak is 2D, at 2660 cm^{-1}, which is the second order of D peak (Krishnamoorthy et al., 2012).

The purity and crystallinity of the graphene were examined by using powder XRD measurement, as shown in Figure 4.2. The graphene multilayers XRD diffraction shows strong and sharp peaks at 26.4°, 43.9°, and 77.4° that can be referred to as the (hkl) crystal structure at (002), (101), and (004), respectively (Yue et al., 2013). The narrow sharp peaks indicate that the graphene is highly crystalline. This implies the high purity of graphene.

4.4.2 Characterizations of Crosslinked NR

The crosslink density of NR films was measured following ASTM D6814-02 and examined under the effects of crosslinking time and crosslinking concentration. Figure 4.3 shows the effect of UV irradiation time on the crosslinking density. When increasing UV-irradiation time, the crosslink density of NR film is dramatically increased. This is because the bonded junction point between each rubber chain increases with UV-irradiation time (Yahya et al., 2011). With longer UV-irradiation time, the photo-initiator and the crosslinker could become more disassociated leading to more possibility to attach with the rubber molecule and causing more crosslinked points within the rubber chain (Choi et al., 2006). However, UV-irradiation time of 15 min. exhibits the lowest crosslink density because high energy

from UV light may create chain scission degradation that can destroy crosslinked points and rubber chains (Kehlet *et al.*).

Furthermore, the crosslink density of NR films, under the condition of concentrations of crosslinker is shown in Figure 4.4. Crosslink density of NR films with various concentrations of crosslinker continuously increases with increasing concentration level due to more possibility to attach with the rubber molecule. This may result from the increase of permanently bonded junction points with increasing crosslinker concentration (Choi *et al.*, 2006). But the crosslink density tends to decrease at crosslinking concentration over 15 %v/v because an over crosslinking agent introduces a heterogeneous crosslinking network, with over-crosslinked domains as a cluster (GonzaÂlez *et al.*, 2005). This domain causes a larger accumulations of defect compared with uniform distribution networks of the crosslinked sites.

Figure 4.5 and 4.6 show the mechanical properties of crosslinked NR films at various UV-irradiation times and concentrations of crosslinker, respectively. Under applied strain, stress increases monotonically because molecules of crosslinked NR films become oriented and re-arranged in the direction of stretching, in which crystallization of material occurs during straining, the process is called strain induced crystallization (Toki, 2014). Furthermore, under applied stain up to the critical point, the material loses elasticity and the stress suddenly drops. The critical point is called the yield strength, it is the point that material can hold the elastic part without any defect. When the strain is larger than the critical point, the material tends to completely deform and can not recover to it original shape and size. This causes the loss of elastic behavior and the viscous part is dominant.

Table 4.1 summarizes the mechanical properties of NR film with various UV-irradiation times of the NR films. The yield strength, yield strain, and modulus increases with increasing UV-irradiation time because when increasing crosslinking time, the crosslink density is increased leading to the material becomes more stiffen. The UV-irradiation time of 12 min. shows the highest value, while UV-irradiation time of 15 min. shows the lowest value when compared with others. The decrease of modulus at a higher UV-irradiation time may have occured from the degradation of rubber molecule during the UV curing (Kehlet *et al.* 2014), where the

color appearance of crosslinked film turned to a yellow-brown color. The result suggests that 15 min. is not appropriate to fabricate a crosslinked NR film.

The film mechanical properties change significantly with concentration of crosslinker, as shown in Figure 4.6 and Table 4.2. The higher concentration is, the greater mechanical properties are obtained. But, the mechanical properties drop off with excessive concentration of crosslinker. The main reason can be related to the distribution of crossliked network. If NR film has a homogeneous junction point, the stress arriving at the connected points will be quickly transferred to the other connecting chains as illistrated in the concentration of crosslinker below 5.0 %v/v. But, at the level of concentration over 5.0 %v/v of crosslinker, significant decreases of the mechanical mechanical properties occur because the molecular motions are more restricted and the stress is not rapidly transferred through NR chains causing some accumulations of stress within some clusters (Lederer *et al.*, 1981). Furthermore, the photoinitiator and crosslinker also bloomed out to the NR film surface that confirms the excessive concentration to crosslink the film. Consequently, the best material performance belongs to the concentration of crosslinker of 5 %v/v which shows the maximum strength of 0.77 MPa and yield strain of 50 %.

4.4.3 Characterizations of Graphene/NR Composite

FE-SEM images of the composites are shown in Table 4.3. The photographs exhibit the dispersion and distribution of graphene multilayers in the NR matrix. The 5.0 %v/v graphene/NR composite have a good dispersion when compared with 20.0 %v/v graphene/NR composite at the same magnification. Moreover, the magnification of 60 kX can be used to confirm the agglomeration of graphene mulltilayers in 20.0%v/v graphene/NR composite.

From topology image of AFM technique, the distributions in microscale of a composite in the area of 2 μm^2 are observed as shown in Figure 4.7. The higher graphene concentration embedded in the NR matrix, the larger agglomeration can be observed. Interestingly, 5.0 %v/v graphene/NR composite exhibits the best dispersion of graphene in the matrix without agglomeration and also shows a uniform dispersion compared with other composites. In contrast, the 20.0 %v/v

graphene/NR composite has a poor dispersion with very large agglomeration of graphene. Nevertherless, the commercial DANFOSS compliant electrode exhibits a perfect dispersion of silver metallic particles within polydimethylsiloxane matrix (Berardi, 2013).

Mechanical properties of graphene/NR composites are shown in Table 4.4 and Figure 4.8. The composite film mechanical properties significantly vary with increasing graphene concentration because graphene acts as a reinforcement to enhance the strength of NR matrix. The 20 %v/v of graphene concentration shows the highest values of strength without any material breakdown. The large surface area of graphene offers much stronger reinforcement effect and causes a greater interfacial interaction between graphene and the NR matrix (Yang *et al.*, 2007). The strength of NR film increases from 0.6 MPa to 9.9 MPa when adding 20 %v/v of graphene, a 1500 % increase in the strength at maximum stress. This observed improvement is higher than that previous literature. For example, multi-walled carbon nanotube/NR composite had an increase in stress of 700 % (Bokobza, 2012). However, the presence of a small amount of reinforcement particle, as 0.01 and 0.1 %v/v of graphene in NR matrix, may not have a significant influence in mechanical properties because the particles do not restrict NR molecular chain movement during stretching (Kueseng *et al.*, 2006). Furthermore, adding a large amount of graphene (over 20.0 %v/v), it behaves like a stifftening material. For the 35.0 %v/v graphene/NR composite, it appeared to breakdown at strain of 13.06 % due to an excessive graphene content embedded in the NR matrix. The large amount of graphene acted as a defect in NR matrix because graphene particles tended to agglomerage and thus provided the phase seperation causing a weak physical interaction between graphene surface and the NR matrix. Moreover, the performance of composite changes form rubbery-like to plastic-like behavior with applied graphene content more than 20.0 %v/v. Thus, this indicates that an increase of graphene concentration directly affects the mechanical properties of composites. Comparing with commercial DANFOSS compliant electrode, over 5.0 %v/v of graphene embedded in NR matrix exhibits a better mechanical performance including yield strength, yield strain, and modulus. Especially for yield strength, these composites show a value higher than that of DANFOSS by a factor of 2.

Figure 4.9 shows the electrical conductivity of composite film under stretching. The electrical conductivity tends to decrease with increasing strain because the distance between graphene particles is longer, when applying a larger strain. The electron pathways are hindered with increasing strain and thus electrical conductivity is dramatically reduced. Moreover, at a critical strain, some of the graphene conductive pathways are permanently damaged by excessive stretching. As a higher graphene content embedded in NR matrix, a greater critical strain is obtained, as shown in Table 4.5, because a larger amount of graphene has a larger number of conductive networks and leading to electrical network breakdown (Cocci *et al.*, 1973).

In addition, electrical conductivity increases with increasing graphene concentration as the electrical conductive pathways from graphene are increased. The electrical conductivity can be divided into 2 groups. For the first group, the 0.01, 0.1, and 1.0 %v/v of graphene contents show very low conductivity because conductive pathway or distance between graphene filler is too large to conduct the electrons along the specimen. The second group, over 5.0 %v/v of graphene concentrations has a higher conductivity because the amount of graphene embedded in rubber matrix is high enough to conduct electrons and the distance between graphene particles is shorter. Therefore, the electrons transfer is easier and the conductivity is greater than the first group. At this concentration, the graphene content reaches the percolation threshold due to the overshoot of electrical conductivity. The 35.0 %v/v graphene concentration exibited the highest conductivity (0.6 S/cm) because the fillers were very close to each other allowing electrons to easily jump and hop along the electrical pathways throughout the specimen (Kim *et al.*, 2012). The electrical conductivity was improved by 4 orders of magnitude whencompared with the pristine rubber. Furthermore, when compared with commercial DANFOSS compliant electrode, for the concentrations of graphene over 10.0 %v/v embedded in NR matrix indcued higher electrical conductivity than the commercial one. Compared with the other conductive fillers, the electrical conductivity of single-walled carbon nanotube/acrylic elastomer composite, carbon black/silicon rubber composite, silver nanopaticle/poly(*tert*-butylacrylate-co-acrylic acid) composite, and carbon nanotube/polyurethane was 0.34 S/cm, 1.7×10^{-4} S/cm, 2.8×10^{-3} S/cm, and 0.1 S/cm, re-

spectively (Kim *et al.*, 2012, Witt *et al.*, 2013, Yun *et al.*, 2012, and Shin *et al.*, 2010).

In order to be used as a compliant electrode, the composites should possess the ability to absorb certain levels of strain without undergoing any significant degradation in their electrical conductivity. Electrical conductivity under stretching cycles is investigated and shown in Figure 4.10. Both of the 0.01 and 5.0 %v/v of graphene concentration composites their electrical conductivity remains nearly constant with increasing stretching cycle. But for 20 %v/v of graphene content, electrical conductivity gradually decreases due to the loss of electrical conductivity pathway (Kujawski *et al.*, 2010). Indeed, when the composites are stretched to 1 % strain for 20 times, the conductivity of all composites drops off. The change in conductivity of 20.0 %v/v graphene/NR composite is much higher than the others in which it decreases by a factor of 1.36 (from 0.33 S/cm to 0.14 S/cm). While 5.0 %v/v graphene/NR composite has a decrease by a factor of 0.1 (from 0.11 S/cm to 0.10 S/cm). This low degradation of electrical conductivity of 5.0 %v/v graphene/NR composite is due to the uniform dispersion of graphene in the NR matrix. During stretching in the first cycle, the conductive pathways are aligned in the direction of strain as a filler orientation. After several stretching, destruction of the electrical pathways slightly occurs (Buselli *et al.*, 2011). But in the case of agglomerated graphene in the matrix, conductive pathways are permanently damaged with weak contacts with neighboring conductive particles, due to excessive one-dimensional stretching that causes a larger conductivity drop under repeated strain (Kim *et al.*, 2012).

The other stretching parameter that affects the conductivity of the composites is the strain rate. As mentioned earlier, during stretching, two possible phenomena can occur which are filler orientation and conductive network breakdown. Beyond the critical strain, the breakage of conductive pathway becomes much more predominant. As shown in Figure 4.11, the critical strain of 5.0 %v/v graphene/NR composite at the strain rates of 0.01 s^{-1}, 0.1 s^{-1}, and 1.0 s^{-1} are 2.01 %, 16.60 %, and 61.35 %, respectively. It is evident that critical strain increases with increasing extension rate because material has a little time for the conductivity response. Hence, the result implies that the faster mobility of composite is responsible

for the decrease in the conductive pathway breakdown and the formation of a few new conductive networks in the NR matrix might be occur (Das *et al.*, 2002).

4.5 Conclusions

Flexible compliant electrode has been prepared by natural rubber (NR) filled with multilayer graphene nanoplatelets. The crosslinked NR films were obtained by the UV crosslink technique. The best crosslinking condition was 7 minute of UV irradiation time and 5.0 %v/v crosslinker concentration, it exhibited the yield strength of 0.77 MPa, yield strain of 50.4 %, and modulus of 0.018 MPa, and with the crosslink density of 7.3×10^{-5} mole/cm^3. In addition, the mechanical property, especially the strength, of NR was improved when adding graphene. The highest electrical conductivity was obtained from the 35.0 %v/v graphene/NR composite (0.6 S/cm). Interestingly, the electrical condcutivity of the 5.0 %v/v graphene/NR composite did not significantly change within 20 stretching cycle times due to a uniform dispersion of graphene in NR matrix. From these results, it can be summarized that 5.0 %v/v graphene/NR composite is an interesting material candidate for use as a compliant electrode with very low conductivity drop under repeating stretching cycles.

4.6 Acknowledgements

4.7 References

Arayapranee, W. and Rempel, G.L. (2008). Morphology and mechanical properties of natural rubber and styrene-grafted natural rubber latex compounds. Journal of Applied Polymer Science, 109(3), 1395-1402.

Berardi, U. (2013). Modelling and testing of a dielectic electro-active polymer (DEAP) actuator for active vibration control. Journal of Mechanical Science and Technology, 27(1), 1-7.

Bhattacharyya, S., Sinturel, C., Bahloul, O., Saboungi, M.-L., Thomas, S. and Salvetat, J.-P. (2008). Improving reinforcement of natural rubber by networking of activated carbon nanotubes. Carbon, 46(7), 1037-1045.

Bokobza, L. (2012). Multiwall carbon nanotube-filled natural rubber: Electrical and mechanical properties. Express Polymer Letters, 6(3), 213-223.

Buselli, E., Smith, A.M., Grover, L.M., Levi, A., Allman, R., Mattoli, V., Menciassi, A. and Beccai, L. (2011). Development and characterization of a bio-hybrid skin-like stretchable electrode. Microelectronic Engineering, 88(8), 1676-1680.

Choi, S.S., Hong, J.P., Seo, Y.S., Chung, S.M. and Nah, C. (2006). Fabrication and characterization of electrospun polybutadiene fibers crosslinked by UV irradiation. Journal of Applied Polymer Science, 101(4), 2333-2337.

Cocci, A.A. and Picot, J.J.C. (1973). Rate of strain effect on the thermal conductivity of a polymer liquid. Polymer Engineering & Science, 13(5), 337-341.

Das, N.C., Chaki, T.K. and Khastgir, D. (2002). Effect of axial stretching on electrical resistivity of short carbon fibre and carbon black filled conductive rubber composites. Polymer International, 51(2), 156-163.

Delille, R., Urdaneta, M., Hsieh, K. and Smela, E. (2006). Novel compliant electrodes based on platinum salt reduction. 61681Q-61681Q.

Ferrari, A.C. (2007). Raman spectroscopy of graphene and graphite: Disorder, electron–phonon coupling, doping and nonadiabatic effects. Solid State Communications, 143(1–2), 47-57.

GonzaÂlez, L., RodrõÂguez, A., ValentõÂn, J.L., Marcos-FernaÂndez, A. and and Po-sadas, P. (2005). Conventional and efficient crosslinking of natural rubber. Elastomers and Plastics,(1), 638-643.

Kehlet, C., Catalano, A. and Dittmer, J. Degradation of natural rubber in works of art studied by unilateral NMR and high field NMR spectroscopy. Polymer Degradation and Stability,(0).

Kim, J.S., Yun, J.H., Kim, I. and Shim, S.E. (2011). Electrical properties of graphene/SBR nanocomposite prepared by latex heterocoagulation process at room temperature. Journal of Industrial and Engineering Chemistry, 17(2), 325-330.

Kim, T.A., Kim, H.S., Lee, S.S. and Park, M. (2012). Single-walled carbon nanotube/silicone rubber composites for compliant electrodes. Carbon, 50(2), 444-449.

Krishnamoorthy, K., Kim, G.-S. and Kim, S.J. (2013). Graphene nanosheets: Ultrasound assisted synthesis and characterization. Ultrasonics Sonochemistry, 20(2), 644-649.

Krishnamoorthy, K., Veerapandian, M., Mohan, R. and Kim, S.-J. (2012). Investigation of Raman and photoluminescence studies of reduced graphene oxide sheets. Applied Physics A, 106(3), 501-506.

Kueseng, K. and Jacob, K.I. (2006). Natural rubber nanocomposites with SiC nanoparticles and carbon nanotubes. European Polymer Journal, 42(1), 220-227.

Kujawski, M., Pearse, J.D. and Smela, E. (2010). Elastomers filled with exfoliated graphite as compliant electrodes. Carbon, 48(9), 2409-2417.

Lederer, D.A. and Fath, M.A. (1981). Effects of Wax and Substituted p-Phenylenediamine Antiozonants in Rubber. Rubber Chemistry and Technology, 54(2), 415-426.

Luong, N.D., Hippi, U., Korhonen, J.T., Soininen, A.J., Ruokolainen, J., Johansson, L.-S., Nam, J.-D., Sinh, L.H. and Seppälä, J. (2011). Enhanced mechanical and electrical properties of polyimide film by graphene sheets via in situ polymerization. Polymer, 52(23), 5237-5242.

Mamunya, Y.P., Davydenko, V.V., Pissis, P. and Lebedev, E.V. (2002). Electrical and thermal conductivity of polymers filled with metal powders. European Polymer Journal, 38(9), 1887-1897.

Manmoun, S. (2013). Para rubber with Asean Economics Community. Para rubber (Rubber Research Institute of Thailand), 34(1), 1-33.

Pelrine, R., Kornbluh, Roy, Pei, Q. and Joseph, J. (2000). High-Speed Electrically Actuated Elastomers with Strain Greater Than 100%. Science, 287(5454), 836-839.

Pramila Devi, D.S., Bipinbal, P.K., Jabin, T. and K.N. Kutty, S. (2013). Enhanced electrical conductivity of polypyrrole/polypyrrole coated short nylon fiber/natural rubber composites prepared by in situ polymerization in latex. Materials & Design, 43(0), 337-347.

Sengupta, R., Bhattacharya, M., Bandyopadhyay, S. and Bhowmick, A.K. (2011). A review on the mechanical and electrical properties of graphite and modified graphite reinforced polymer composites. Progress in Polymer Science, 36(5), 638-670.

Shin, M.K., Oh, J., Lima, M., Kozlov, M.E., Kim, S.J. and Baughman, R.H. (2010). Elastomeric Conductive Composites Based on Carbon Nanotube Forests. Advanced Materials, 22(24), 2663-2667.

Sincharoenkul, C.R.A.O.T. (2012). "Para rubber situation in 2013." Retrieved December, 2012, from http://www.thainr.com/th/message_detail.php?MID= 187.

Toki, S. (2014). 5 - The effect of strain-induced crystallization (SIC) on the physical properties of natural rubber (NR). Chemistry, Manufacture and Applications of Natural Rubber, Kohjiya, S. and Ikeda, Y., Woodhead Publishing: 135-167.

Wang, X., Zhi, L. and Mullen, K. (2007). Transparent, Conductive Graphene Electrodes for Dye-Sensitized Solar Cells. Nano Letters, 8(1), 323-327.

Witt, N., Tang, Y., Ye, L. and Fang, L. (2013). Silicone rubber nanocomposites containing a small amount of hybrid fillers with enhanced electrical sensitivity. Materials & Design, 45(0), 548-554.

Yahya, Y.S.R., Azura, A.R. and and Ahmad, Z. (2011). Effect of Curing Systems on Thermal Degradation Behaviour of Natural Rubber (SMR CV 60). Journal of Physical Science, 22(2), 1–14.

Yang, J., Tian, M., Jia, Q.-X., Shi, J.-H., Zhang, L.-Q., Lim, S.-H., Yu, Z.-Z. and Mai, Y.-W. (2007). Improved mechanical and functional properties of

elastomer/graphite nanocomposites prepared by latex compounding. <u>Acta Materialia</u>, 55(18), 6372-6382.

Yue, G., Wu, J., Xiao, Y., Lin, J., Huang, M., Lan, Z. and Fan, L. (2013). Functionalizedgraphene/poly(3,4ethylenedioxythiophene): polystyrenesulfonate as counter electrode catalyst for dye-sensitized solar cells. <u>Energy</u>, 54(0), 315-321.

Yun, S., Niu, X., Yu, Z., Hu, W., Brochu, P. and Pei, Q. (2012). Compliant Silver Nanowire-Polymer Composite Electrodes for Bistable Large Strain Actuation. <u>Advanced Materials</u>, 24(10), 1321-1327.
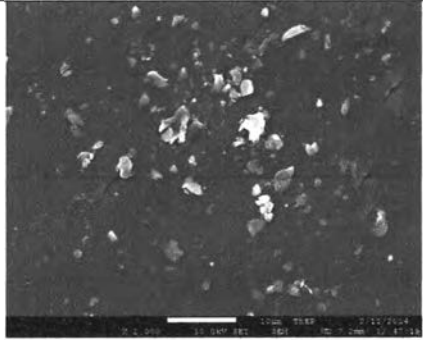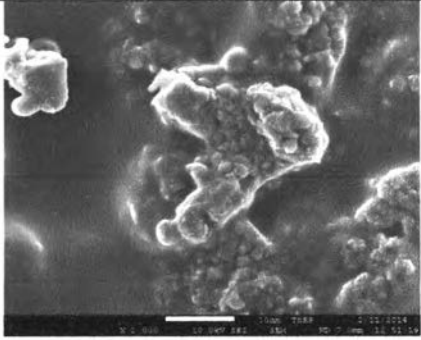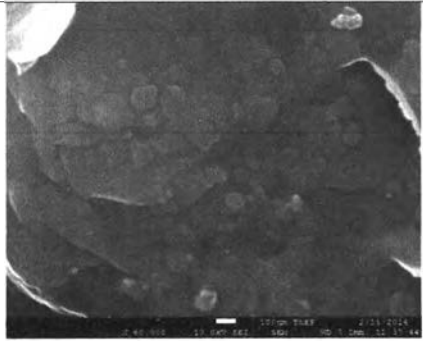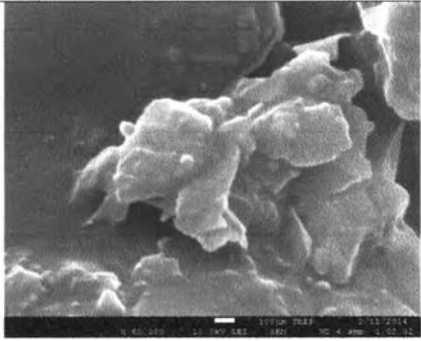
Table 4.1 Mechanical properties of NR films at various UV-irradiation times, a fixed concentration of crosslinker of 2.0 %v/v, by using the melt rheometer in the tension mode with a strain rate 0.01 s^{-1} and temperature of 300 K

UV-irradiation times (min)	Yield strength (Pa)	Yield strain (%)	Modulus (Pa)
0	2.65E+5 ± 9.27E+4	53.97 ± 7.39	4.67E+3 ± 1.0E+3
7	4.92E+5 ± 1.12E+5	70.39 ± 7.26	6.82E+3 ± 8.74E+2
12	8.62E+5 ± 1.70E+5	73.61 ± 2.09	1.16E+4 ± 1.75E+2
15	3.23E+5 ± 9.67E+3	62.23 ± 4.28	5.05E+3 ± 5.06E+2

Table 4.2 Mechanical properties of NR films at various concentrations of crosslinker, a fixed UV-irradiation time of 7 min., by using the melt rheometer in the tension mode with a strain rate 0.01 s^{-1} and temperature of 300 K

Concentrations of crosslinker (%v/v)	Yield strength (Pa)	Yield strain (%)	Modulus (Pa)
0.1	3.09E+5 ± 9.00E+4	45.02 ± 9.17	7.76E+3 ± 7.00E+2
0.5	3.41E+5 ± 6.00E+4	36.76 ± 3.37	1.00E+4 ± 1.09E+2
1.0	5.53E+5 ± 5.37E+3	46.80 ± 3.20	1.29E+4 ± 9.82E+2
2.0	4.92E+5 ± 1.12E+5	51.57 ± 5.84	1.06E+4 ± 1.36E+3
3.0	5.25E+5 ± 1.40E+5	39.58 ± 6.07	1.30E+4 ± 2.20E+3
5.0	7.71E+5 ± 2.04E+5	50.41 ± 5.18	1.79E+4 ± 1.27E+3
7.0	5.08E+5 ± 1.11E+5	39.18 ± 2.74	1.16E+4 ± 3.93E+2
10.0	6.29E+5 ± 1.22E+5	45.46 ± 3.18	1.32E+4 ± 1.08E+3
15.0	7.44E+5 ± 1.15E+5	50.30 ± 4.98	1.54E+4 ± 1.69E+3
20.0	6.71E+5 ± 5.81E+4	53.66 ± 5.82	1.96E+4 ± 3.02E+3

Table 4.3 FE-SEM images of the 5.0%v/v graphene/NR composite and the 20.0%v/v graphene/NR composite at different magnifications

| Magnification	FE-SEM images	
	5.0%v/v graphene/NR composite	20.0%v/v graphene/NR composite
2 kX		
60 kX		

Table 4.4 Mechanical properties of graphene/NR composites at various concentrations of the graphene multilayers as measured by the melt rheometer in the tension mode with a strain rate of $0.01\ s^{-1}$, temperature of 300 K, and applied electric field of 5 volt

Graphene concentration (%v/v)	Yield strength (Pa)	Yield strain (%)	Modulus (Pa)
0.0	6.14E+5 ± 1.18E+5	63.60 ± 2.04	4.75E+4 ± 399.45
0.01	6.26E+5 ± 3.28E+4	70.23 ± 2.42	8.48E+3 ± 497.65
0.1	4.07E+5 ± 1.04E+5	54.87 ± 1.88	5.95E+3 ± 401.56
1.0	7.11E+5 ± 2.76E+4	66.46 ± 2.29	7.12E+3 ± 32.10
5.0	8.36E+6 ± 4.18E+5	69.86 ± 3.49	1.13E+5 ± 5.67E+4
10.0	9.15E+6 ± 4.57E+5	53.53 ± 2.67	1.63E+5 ± 8.15E+4
20.0	9.99E+6 ± 4.99E+5	60.42 ± 3.00	1.54E+5 ± 7.71E+4
30.0	4.95E+6 ± 2.47E+5	16.75 ± 0.84	2.66E+5 ± 1.33E+4
35.0	4.36E+6 ± 2.18E+5	13.06 ± 0.65	2.46E+5 ± 1.23E+4
40.0	3.65E+6 ± 1.82E+5	2.46 ± 0.12	6.99E+5 ± 3.50E+4
45.0	5.94E+6 ± 2.97E+5	1.44 ± 0.07	3.65E+6 ± 1.83E+5
DANFOSS	2.84E+6 ± 1.78E+4	75.12 ± 2.60	8.15E+3 ± 1893.50

Table 4.5 Electrical conductivity of graphene/NR composites at various concentrations of the graphene multilayers as measured by the melt rheometer in the tension mode with a strain rate of 0.01 s^{-1}, temperature of 300 K, and applied electric field of 5 volt

Graphene concentration (%v/v)	Conductivity before stretching (S/cm)	Critical strain* (%)
0.0	1.41E-5 ± 5.47E-6	> 100
0.01	3.55E-5 ± 1.77E-6	> 100
0.1	4.05E-5 ± 2.03E-6	> 100
1.0	3.84E-4 ± 2.23E-4	> 100
5.0	1.10E-1 ± 5.50E-3	2.01 ± 0.11
10.0	1.50E-1 ± 5.07E-2	3.11 ± 0.51
20.0	3.36E-1 ± 1.90E-2	5.02 ± 0.67
30.0	6.04E-1 ± 1.00E-2	12.70 ± 0.92
35.0	6.12E-1 ± 3.06E-2	0.88 ± 0.04
40.0	5.22E-1 ± 2.61E-2	0.23 ± 0.01
45.0	4.86E-1 ± 2.43E-2	0.07 ± 3.64E-3
DANFOSS	2.54E-2 ± 1.27E-3	6.45 ± 0.32

* Critical strain refers to 5% conductivity drop. Beyond this critical strain point, the material's behavior is non-linear and the conductivity declines.
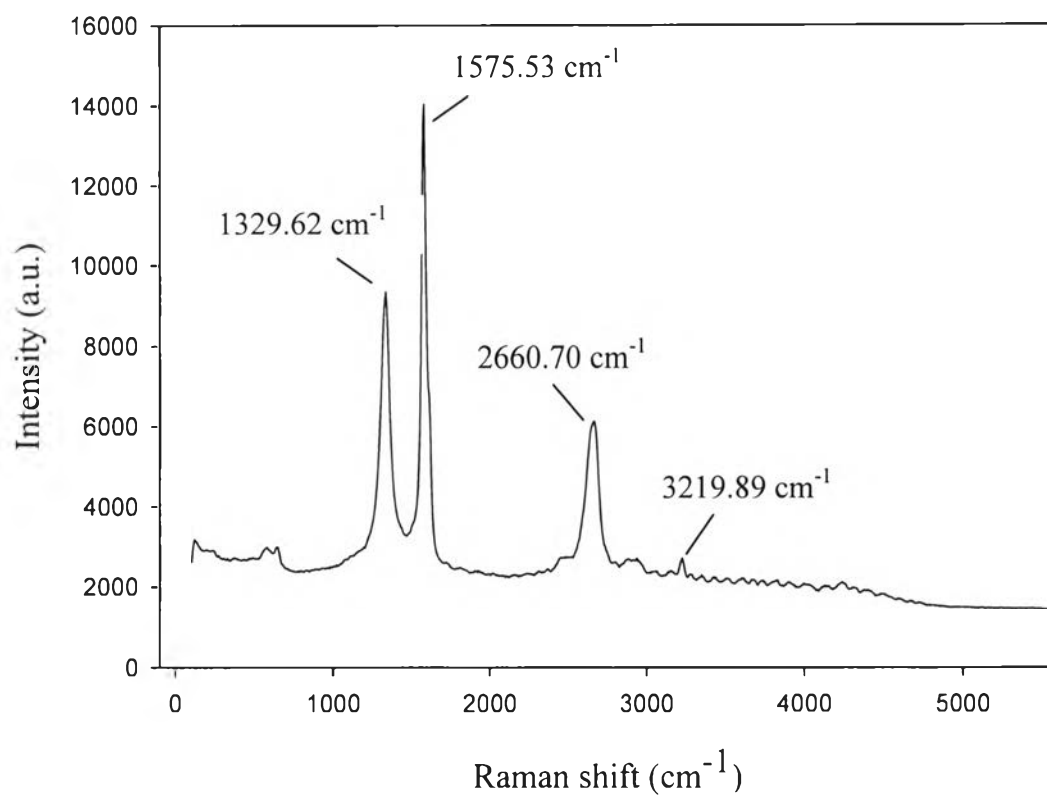
Figure 4.1 Raman spectra of graphene multilayers.
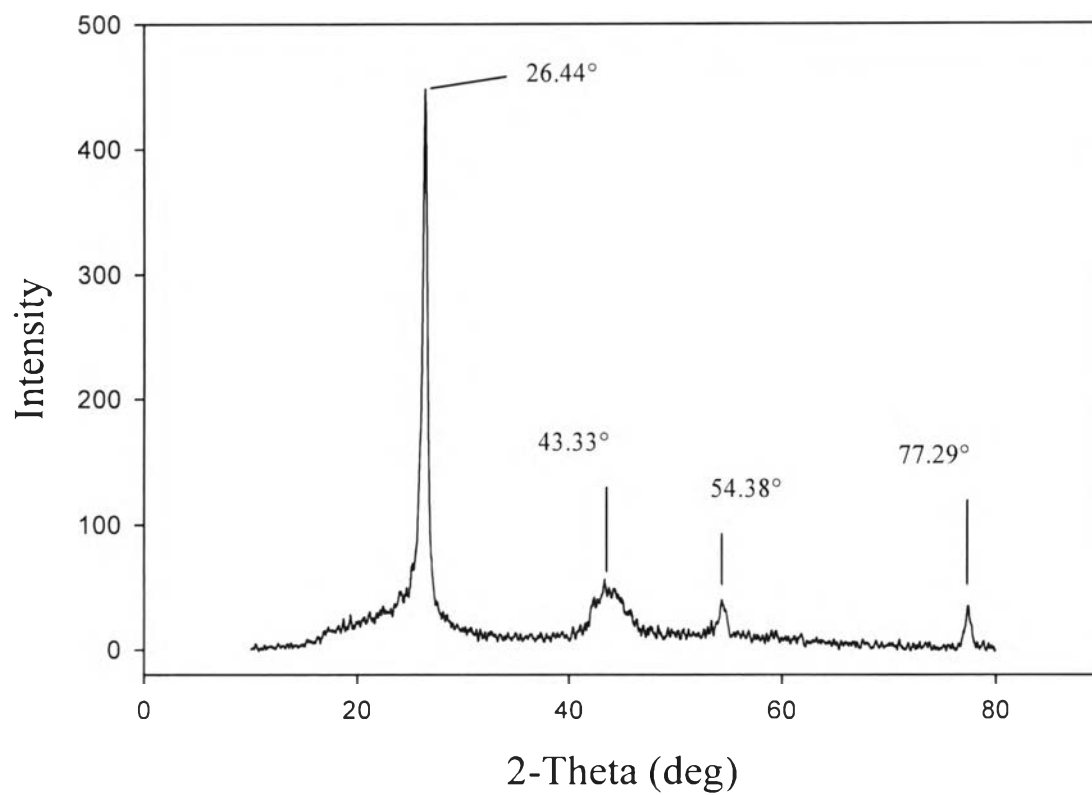
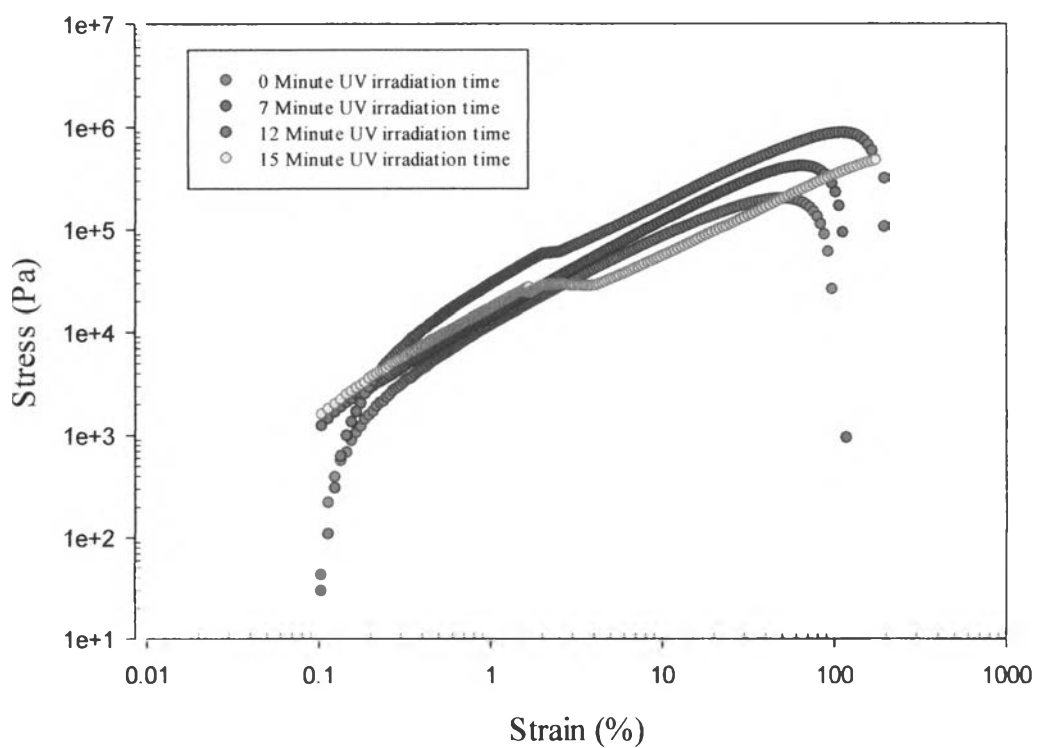**Figure 4.2** XRD pattern of the graphene multilayers.
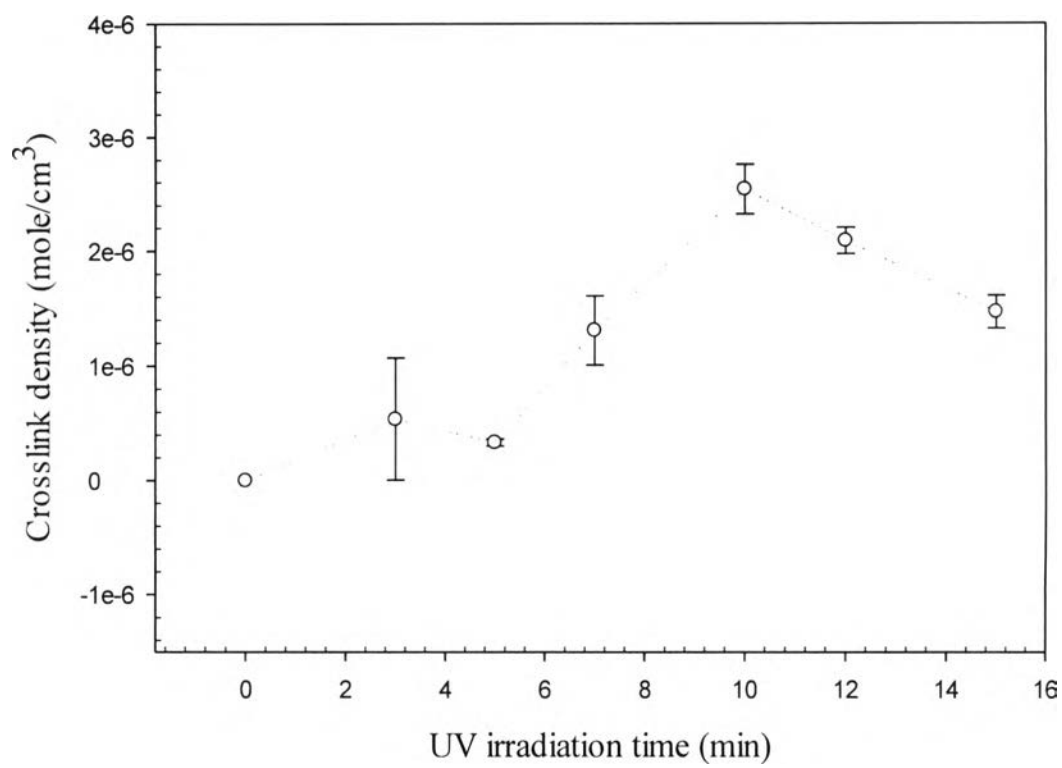
Figure 4.3 Crosslinking density of crossliked NR film at various crosslinking times, a fixed crosslink concentration of 2.0 %v/v.
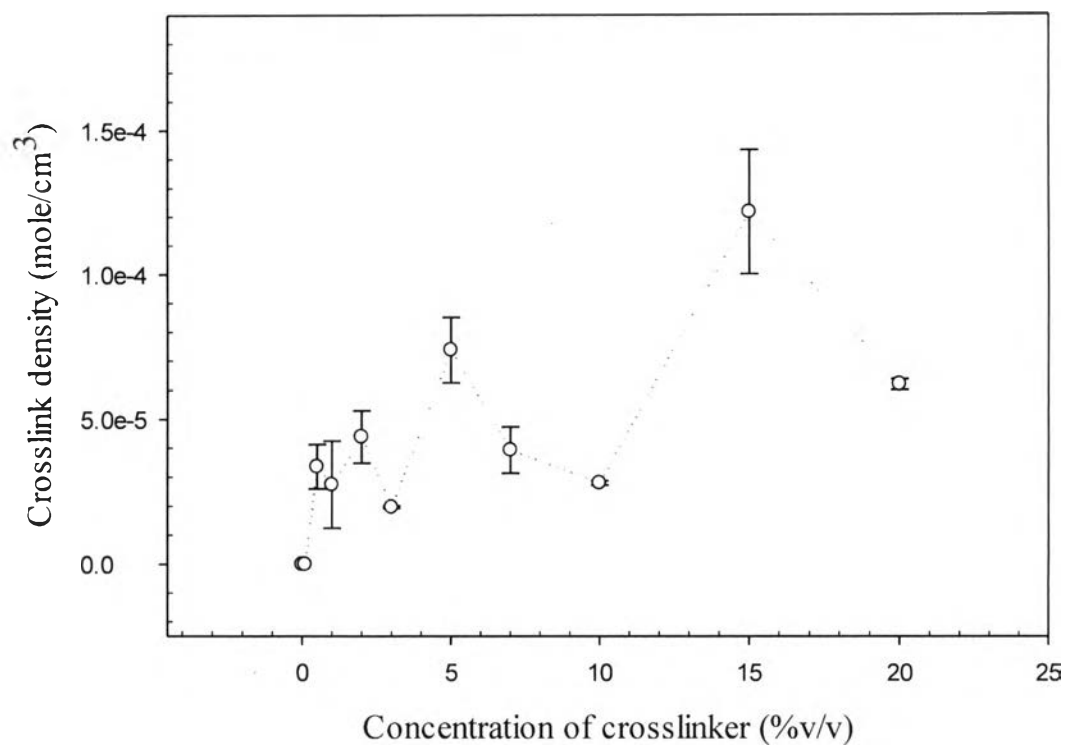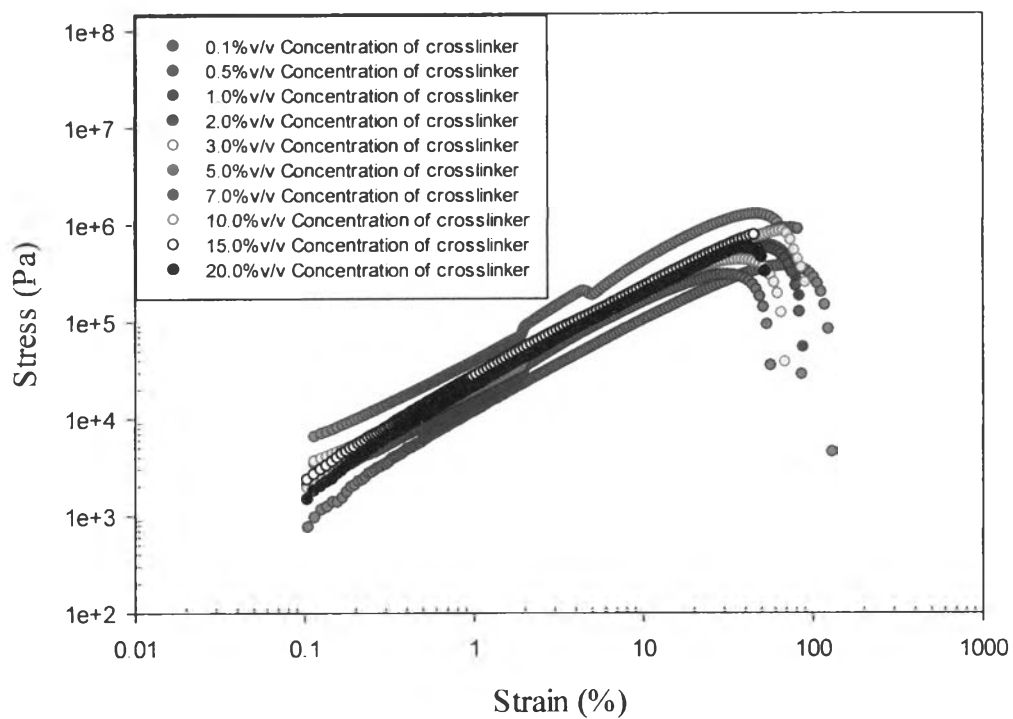
Figure 4.4 Crosslink density of crossliked NR film at various concentrations of crosslinker, and at a fixed UV-irradiation time of 7 min.
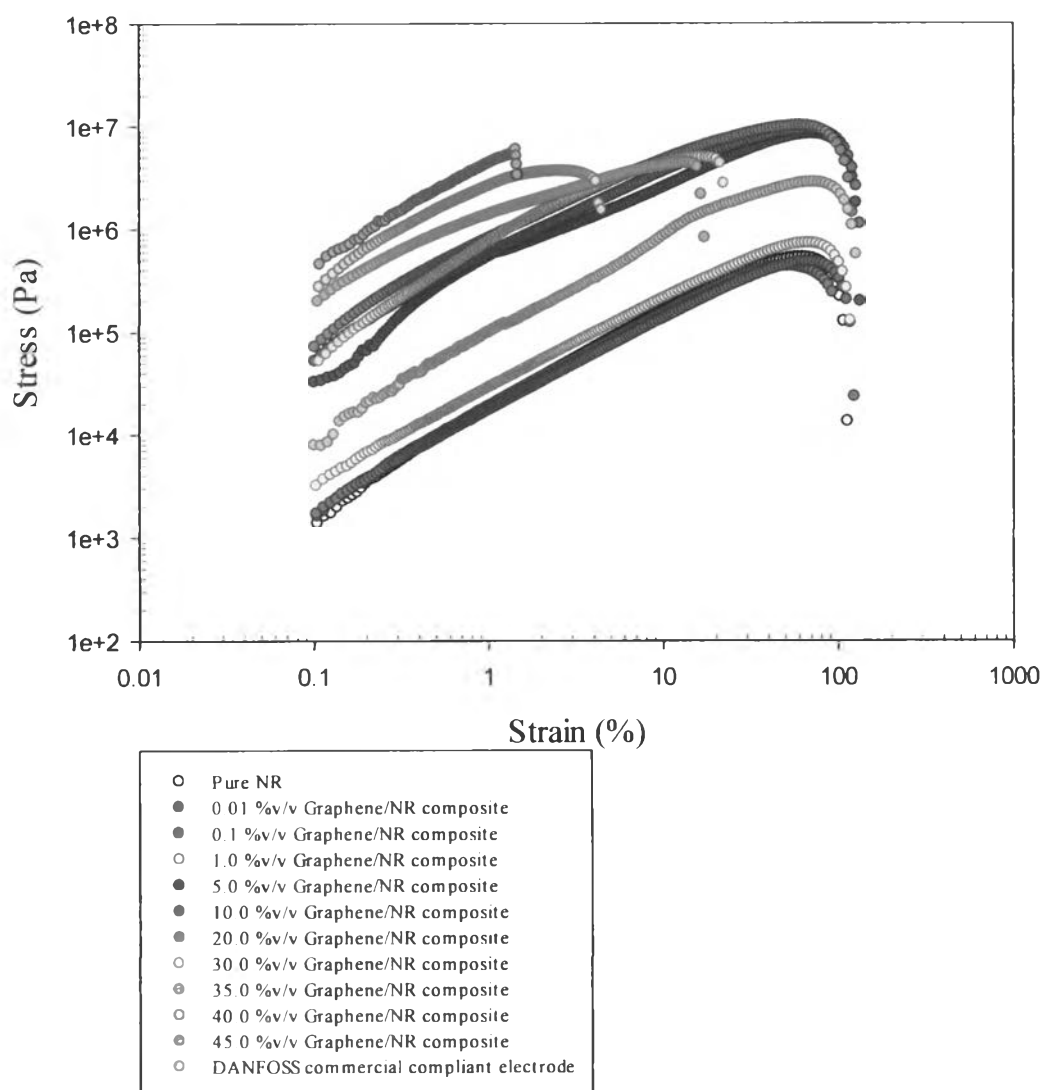
Figure 4.5 Stress-strain curve of NR film at various UV-irradiation times, a fixed concentration of crosslinker of 2.0 %v/v, by using the melt rheometer in the tension mode with a strain rate 0.01 s^{-1} and temperature of 300 K.

Figure 4.6 Stress-strain curve of NR film of various concentrations of crosslinker, a fixed UV-irradiation time of 7 min, by using the melt rheometer in the tension mode with a strain rate 0.01 s^{-1} and temperature of 300 K.
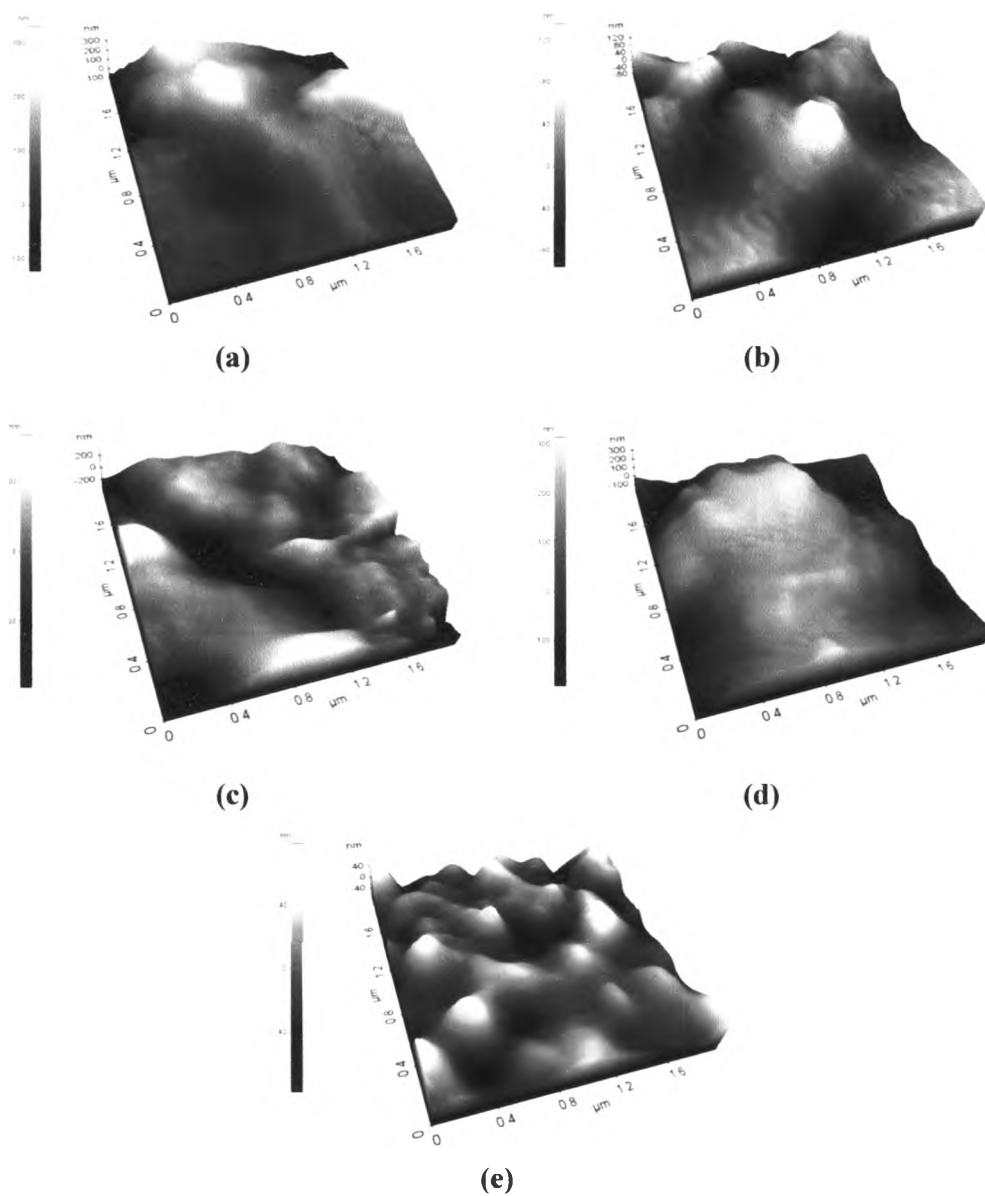
Figure 4.7 Distribution in micro-scale of composite in the area of 2 μm^2 :

(a) 1.0%v/v graphene/NR composite; (b) 5.0%v/v graphene/NR composite;

(c) 10.0%v/v graphene/NR composite; (d) 20.0%v/v graphene/NR composite; and

(e) DANFOSS commercial compliant electrode.

Figure 4.8 Stress-strain curve of graphene/NR composites at various concentrations of the graphene multilayers as measured by the melt rheometer in the tension mode with a strain rate of $0.01s^{-1}$, temperature of 300 K, and applied electric field of 5 volt.
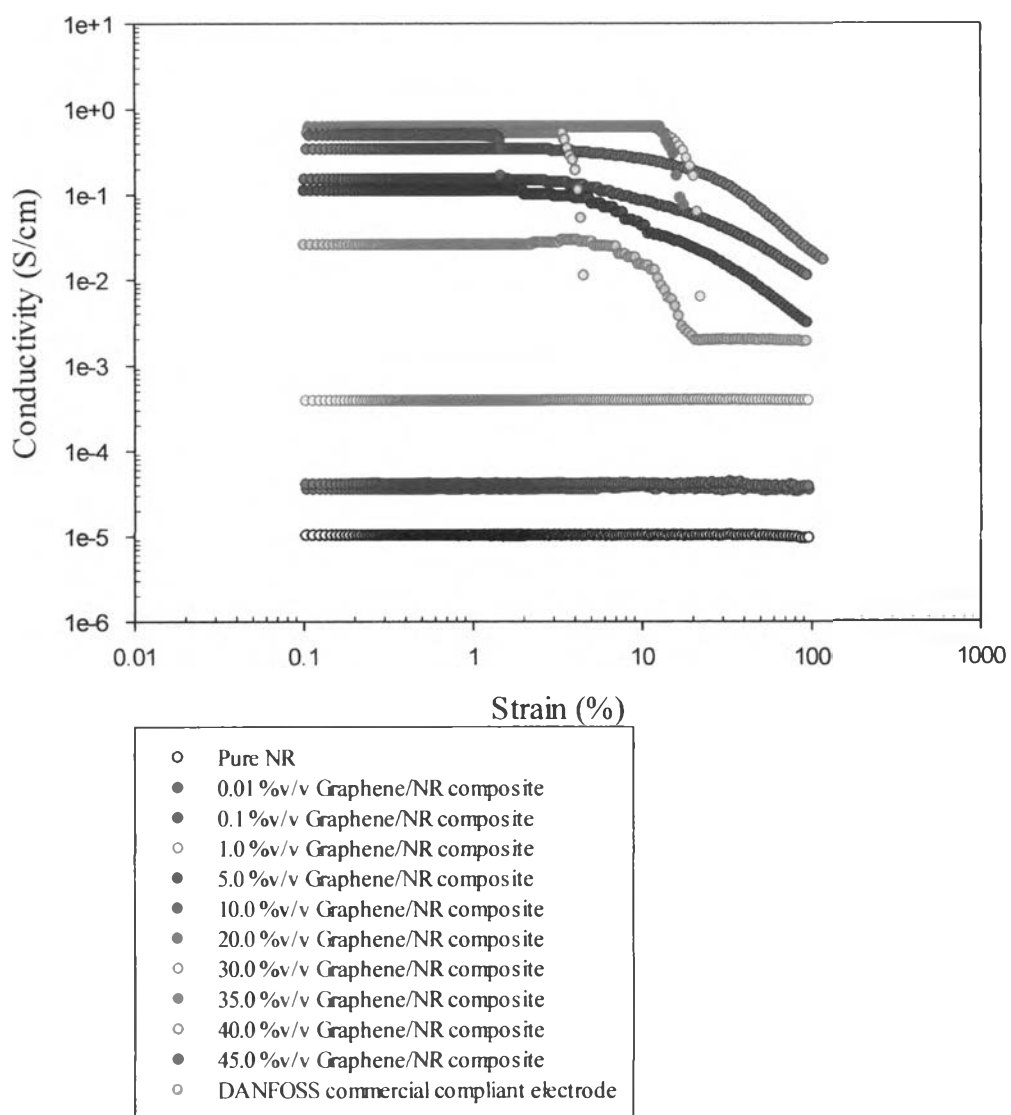
Figure 4.9 Conductivity of graphene/NR composites at various concentrations of the graphene multilayers as measured by the melt rheometer in the tension mode with a strain rate of 0.01 s^{-1}, temperature of 300 K, and applied electric field of 5 volt.
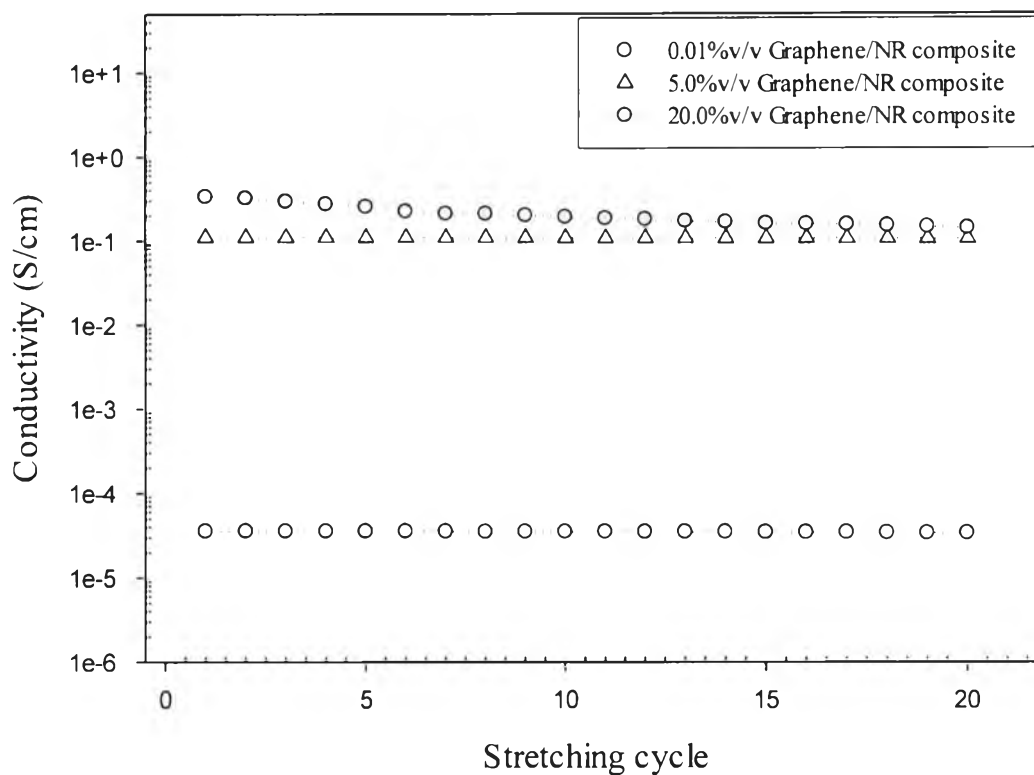
Figure 4.10 Conductivity of the graphene/NR composites as a function of stretching cycles at fixed strain 1% as measured by the melt rheometer in the tension mode with a strain rate of $0.01s^{-1}$, temperature of 300 K, and applied electric field of 5 volt.
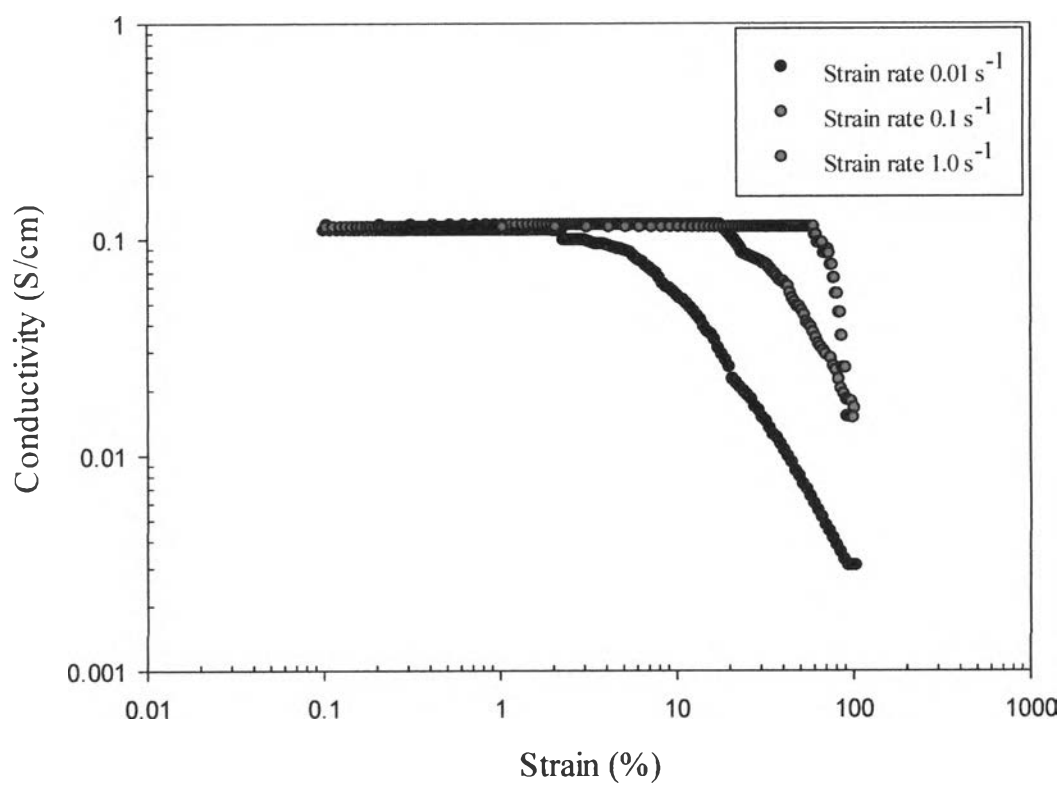
Figure 4.11 Conductivity of 5.0 %v/v graphene/NR composites as a function of strain rate as measured by the melt rheometer in the tension mode with a strain rate of $0.01s^{-1}$, temperature of 300 K, and applied electric field of 5 volt.